Supporting Information

# Water sensitivity of heteroepitaxial Cu-MOF films: dissolution and re-crystallization of 3D-oriented MOF superstructures

*Lea A. Brandner, Mercedes Linares-Moreau, Guojun Zhou, Heinz Amenitsch, Simone Dal Zilio, Zhehao Huang, Christian Doonan*, Paolo Falcaro**

* Corresponding authors: paolo.falcaro@tugraz.at, christian.doonan@adelaide.edu.au

## Experimental



## Supporting Figures

## Supporting Tables



## Supporting Movies

**Movie S1** (.mp4 format): Time-resolved GIWAXS out-of-plane patterns collected during exposure of a $Cu_2(BDC)_2DABCO$ film to a humidity ramp of 10%/min until reaching a target value of 80% RH (held for a total of 25 min).

**Movie S2** (.mp4 format): Time-resolved AFM amplitude and phase images collected during exposure of a $Cu_2(BDC)_2DABCO$ film to a humid environment (80% RH in Ar flow) in a 2×2 $\mu m^2$ area with a scan rate of 9 Hz (2 frames per minute) and a total time of 1h 40m. The video is sped up to 5 fps for a better visualization of the kinetics. We note that at certain frames some of the newly formed particles are removed due to the interaction with the AFM probe.

## Experimental

**Time-resolved GIWAXS measurements under controlled humidity**

$Cu_2(BDC)_2DABCO$ films deposited on Si wafers (1.5 x 1.5 $cm^2$) were synthesized as described and stored under $N_2$ until measurement. At the SAXS beamline, the samples were placed in the customized humidity chamber.[1] Prior to the insertion of the samples, the chamber was dried to < 5% RH to minimize uncontrolled exposure to water molecules before the start of the experiment. Sample alignment was performed under dry conditions (RH< 5%). Then, the in-situ GIWAXS measurements were conducted: 1) a reference frame was recorded at low humidity (LH, < 5% RH), 2) a humidity ramp from LH to the target humidity was applied, 3) structural changes were monitored until a plateau was reached (at least 30 min) at the target RH value (e.g. RH = 50%, 80%, 90%). For the experiments at RH = 50% and 80%, humidity was increased with a rate of 10%/min until the target value was reached. For the measurement

with increasing humidity from 5 to 90% RH, a rate of 0.2%/min was applied. Target and real humidity values were recorded and matched to the timestamps of the collected GIWAXS data. 2D diffraction patterns were recorded every 60 s, using an exposure time of 2 s. After the time-resolved measurement, GIWAXS patterns of two different sample regions, located 2 mm to the right and to the left of the investigated area, were collected and compared to the last frame of the time-resolved measurement. This procedure was performed to assess possible radiation damage related to prolonged exposure of the same area during the time-resolved measurement. For peak position analysis, diffraction peaks were fitted using a Pseudo-Voigt function, defined as follows:

$$f(q) = B + I\left(\eta \cdot a_G \cdot e^{-b_g(q-q_0)^2}\right) + (1-\eta)\,\frac{1}{\pi} \cdot \frac{FWHM}{4\,(q-q_0)^2 + FWHM^2} + a \cdot q + b \cdot q^2$$

with background intensity B, peak intensity I, mixing parameter for Lorentz and Gaussian function $\eta$ (Gaussian ratio, $0 \le \eta \le 1$), peak position q0, peak full with half maximum FWHM, a and b coefficients of the quadratic background and the parameters ag and bg of the Gaussian peak:

$$a_g = \frac{2}{FWHM} \cdot \sqrt{\frac{\ln 2}{\pi}},$$

$$b_g = \frac{4 \cdot \ln 2}{FWHM^2}.$$

**Time-resolved GIWAXS measurements in $H_2O$**

$Cu_2(BDC)_2DABCO$ films deposited on Si wafer (1.5 x 1.5 $cm^2$) were synthesized as described above and stored under $N_2$ until measurement. After sample alignment to the incident beam, a reference frame was recorded in the dry chemical cell.[2,3] Then, water was infused until the cell was filled using a flow rate of 0.5 mL $H_2O$/min. 2D images were recorded every 1.1 s, using a 1 s exposure time for each frame. After recording diffraction patterns for a 15 min period, previously described control measurements to detect potential radiation damage were performed.

**GIWAXS measurements using a rotating stage**

$Cu_2(BDC)_2DABCO$ films deposited on Si wafer (1.5 x 1.5 $cm^2$) were synthesized as described and stored under $N_2$ until measurement. At the beamline, the samples were placed on a motorized stage. The sample insertions were conducted, defining both position and orientation of the MOF films. After the sample alignment to the incident beam, the stage was rotated along the azimuthal angle in the range 0 ° < ϕ < 180 ° and GIWAXS patterns were recorded in 1 ° steps (rotation axis perpendicular to the film surface). Azimuthal intensity profiles were then constructed by integration of the peak of interest ((100) reflections of the 2D and 3D frameworks) over 180 °.

**Synthesis of MOF films for TEM characterization**

$Cu_2(BDC)_2DABCO$ films deposited on Si wafer (1.5 x 1.5 $cm^2$) were synthesized as described and stored under Ar until measurement. The samples, depicting an intermediate state and the full transformation of $Cu_2(BDC)_2DABCO$ to $Cu_2(BDC)_2$ were prepared by exposing fresh $Cu_2(BDC)_2DABCO$ films to 80% RH for 10 min (intermediate state) and 3 h (full conversion).

The films were then washed with dichloromethane (3 x 10 min), evacuated for 30 min and stored under inert conditions (i. e. Ar atmosphere) until measurement.

**Syntheses of powdery samples**

Pristine $Cu_2(BDC)_2$ powder: 5 mL of an ethanolic dispersion of $Cu(OH)_2$nanobelts (ca. 0.36 mmol, 1 eq) were centrifuged and the wet solid dispersed in a solution of 64 mg $H_2BDC$ (0.38 mmol, 1.06 eq) in 23 mL $H_2O$ and 60 mL EtOH. After 30 min at RT, the MOF powder was centrifuged and washed with EtOH (3 x 10 mL).

Pristine $Cu_2(BDC)_2$DABCO powder: 5 mL of an ethanolic dispersion of $Cu(OH)_2$nanobelts (ca. 0.36 mmol, 1 eq) were centrifuged and the wet solid dispersed in 45 mL of a methanolic solution of $H_2BDC$ (7.7 mM) and DABCO (31 mM). After leaving the reaction mixture at 70 °C for 1 h, the MOF powder was centrifuged and washed with MeOH (3 x 10 mL).

Transformed $Cu_2(BDC)_2$ powder: The synthesis procedure of $Cu_2(BDC)_2$DABCO powder was performed. For the transformation, the powder was additionally washed with $H_2O$ (3 x 10 mL - triggering the transformation), and EtOH (3 x 10 mL).

## Supporting Figures

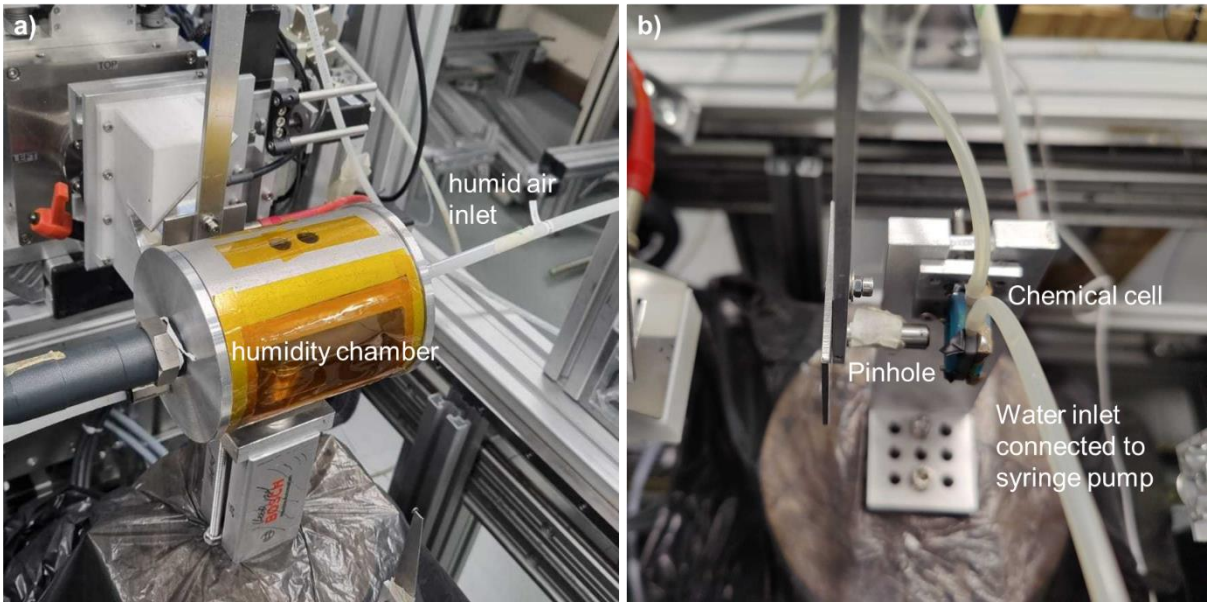


**Fig. S 1:** GIWAXS setups at Austrian SAXS beamline at Elettra. **a)** Humidity chamber and **b)** chemical cell setup.

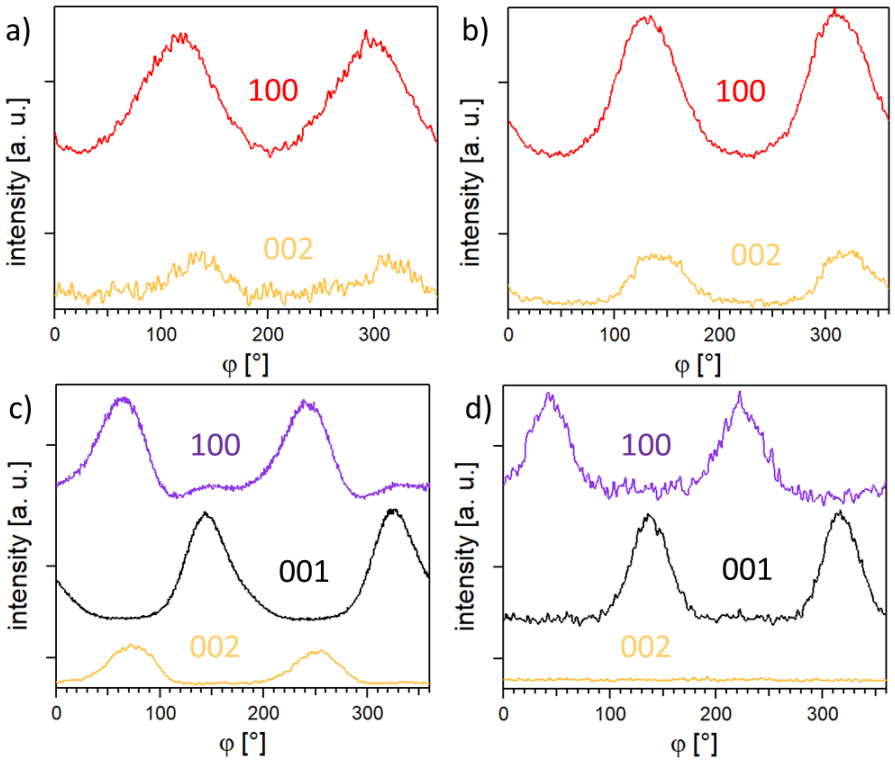


**Fig. S 2:** IP-XRD azimuthal intensity profiles of **a)** the (100) reflection of $Cu_2(BDC)_2$ and the (002) reflection of $Cu(OH)_2$, **b)** the (100) reflection $Cu_2(BPDC)_2$ and the (002) reflection of $Cu(OH)_2$, **c)** the (100) and (001) reflection $Cu_2(BDC)_2DABCO$ and the (002) reflection of $Cu(OH)_2$, **d)** the (100) and (001) reflection $Cu_2(BPDC)_2DABCO$ and the (002) reflection of $Cu(OH)_2$

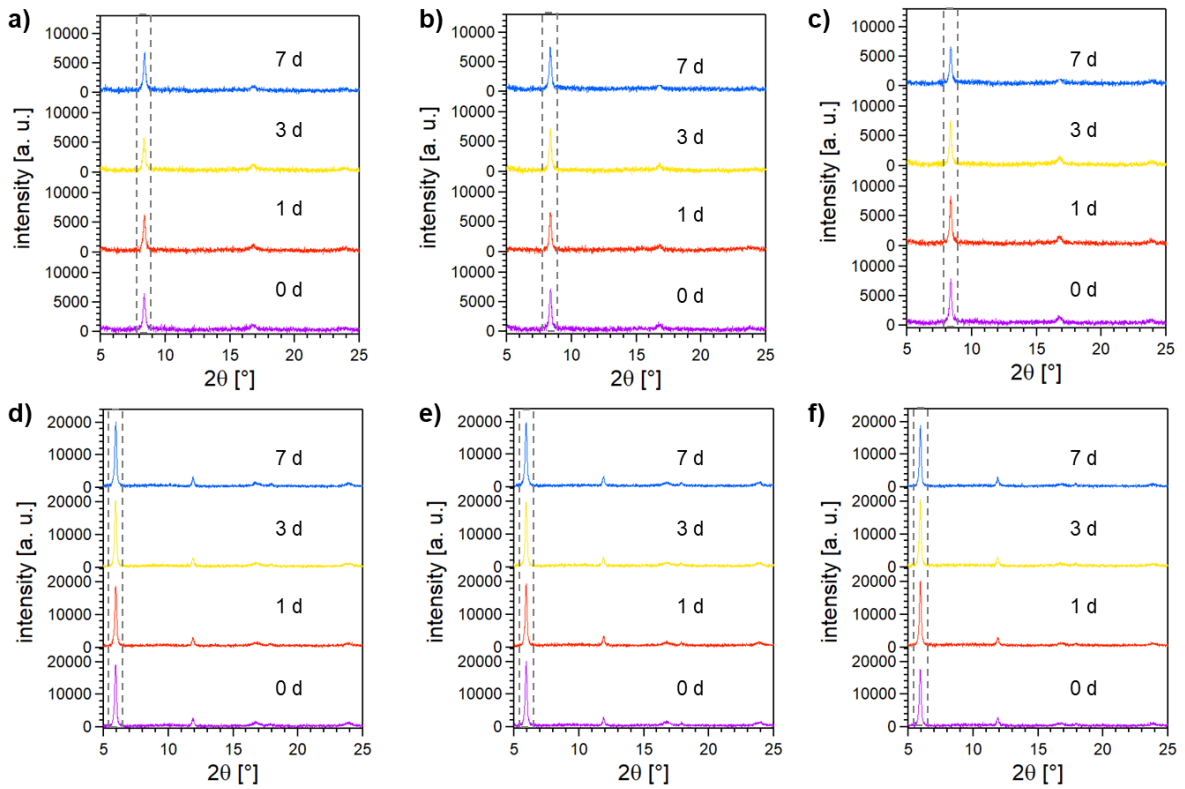


**Fig. S 3:** XRD patterns of representative $Cu_2(BDC)_2$ and $Cu_2(BPDC)_2$ films: $Cu_2(BDC)_2$ exposed to **a)** 50% RH, **b)** 80% RH, **c)** liquid $H_2O$, and $Cu_2(BPDC)_2$ films exposed to **d)** 50% RH, **e)** 80% RH, and **f)** liquid $H_2O$. The (001) reflection of the respective MOF films is highlighted in the box with dashed lines.

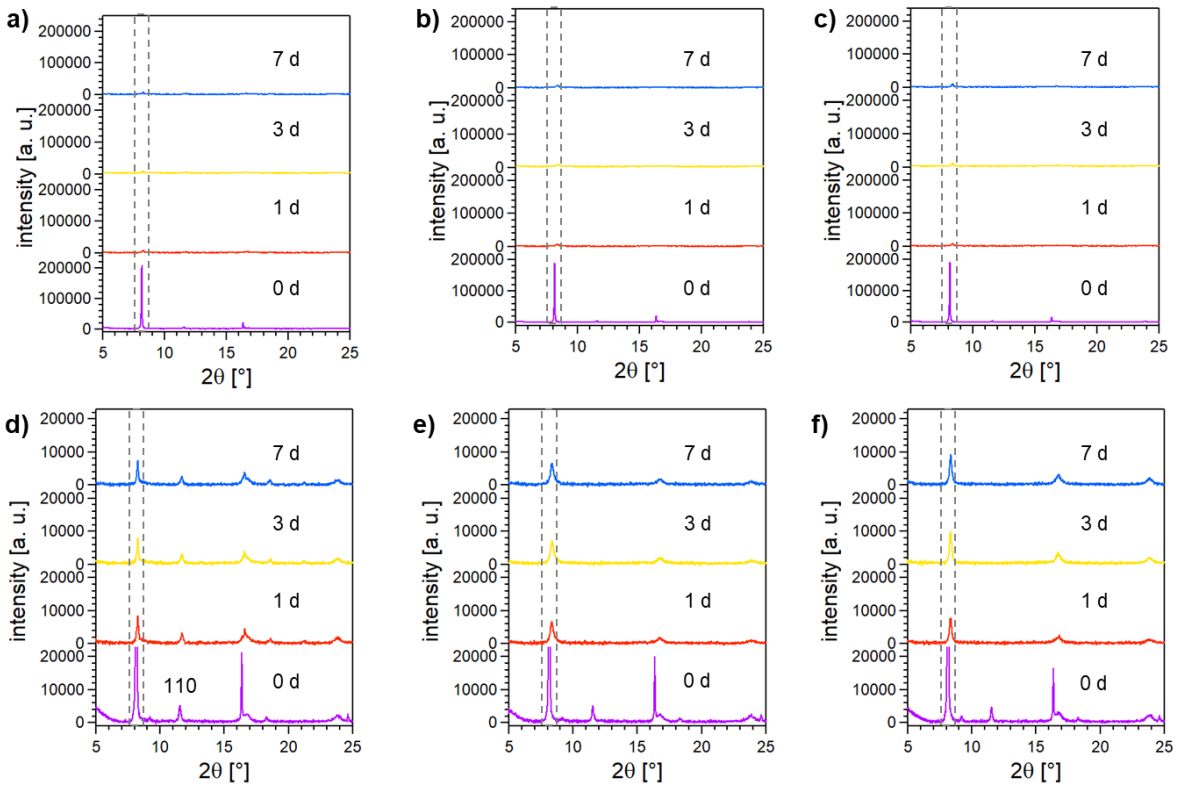


**Fig. S 4:** XRD patterns of representative $Cu_2(BDC)_2DABCO$ films exposed to **a)** 50% RH, **b)** 80% RH, **c)** liquid $H_2O$, and zoom-ins of the same patterns for **d)** 50% RH, **e)** 80% RH, and **f)** liquid $H_2O$. The (010) reflection of the MOF films is highlighted in the box with dashed lines.

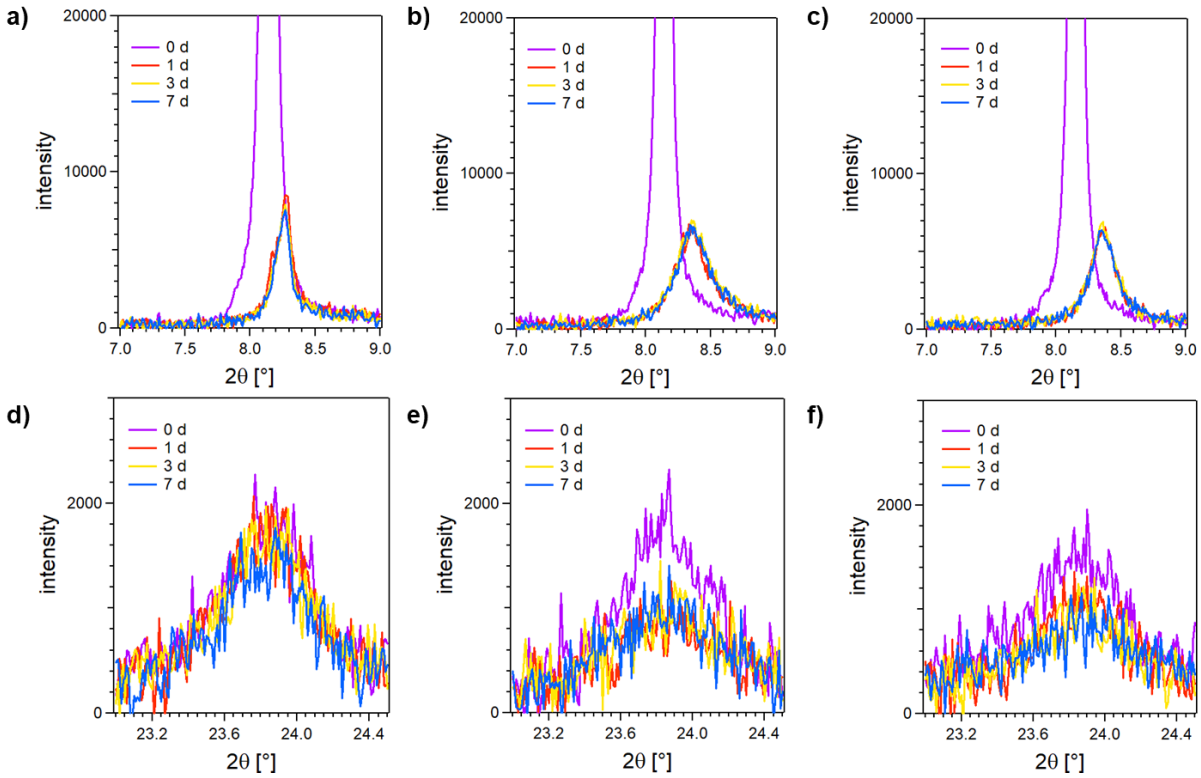


**Fig. S 5:** Evolution of selected reflections of heteroepitaxial $Cu_2(BDC)_2DABCO$ films: (001) after 24 h exposure to **a)** 50% RH, **b)** 80% RH, **c)** liquid $H_2O$, and (021) reflection of remaining $Cu(OH)_2$ in the heteroepitaxially grown MOF films after 24 h exposure to **d)** 50% RH, **e)** 80% RH, and **f)** liquid $H_2O$.

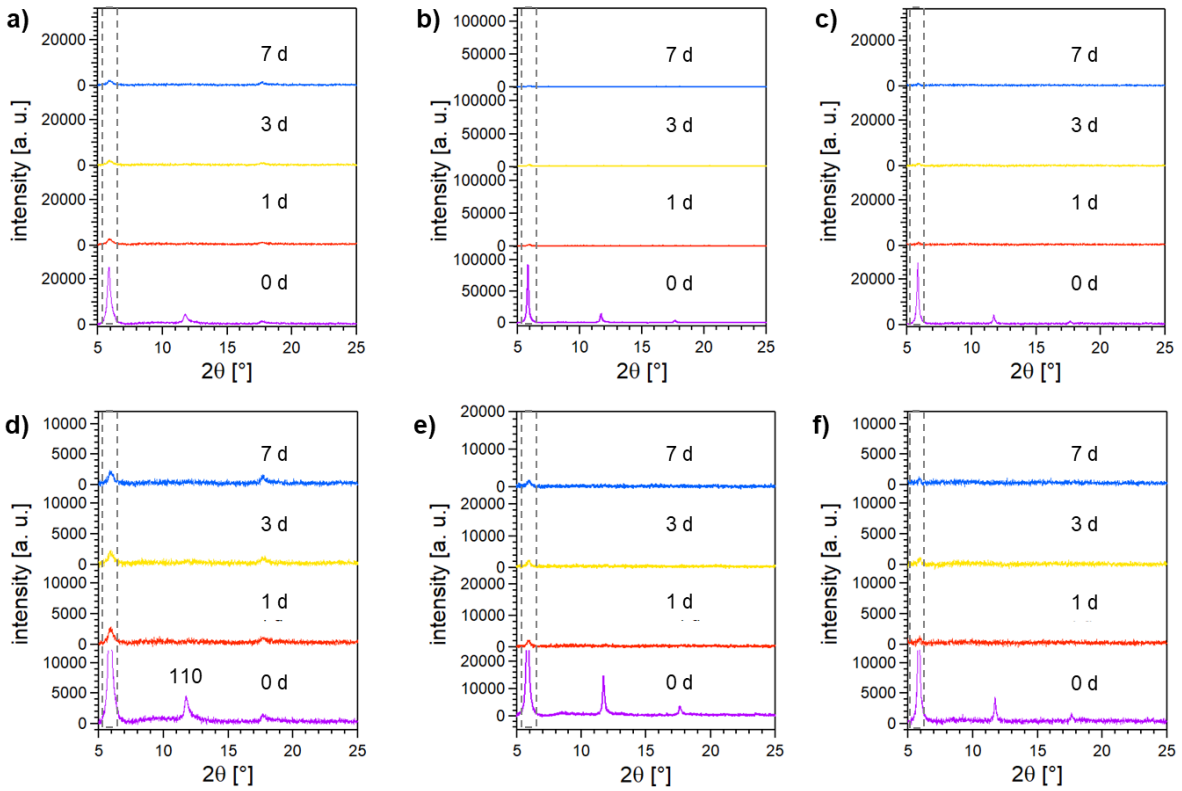


**Fig. S 6:** XRD patterns of representative $Cu_2(BPDC)_2DABCO$ films exposed to **a)** 50% RH, **b)** 80% RH, **c)** liquid $H_2O$, and zoom-ins of the same patterns for **d)** 50% RH, **e)** 80% RH, and **f)** liquid $H_2O$. The (010) reflection of the MOF films is highlighted in the box with dashed lines.

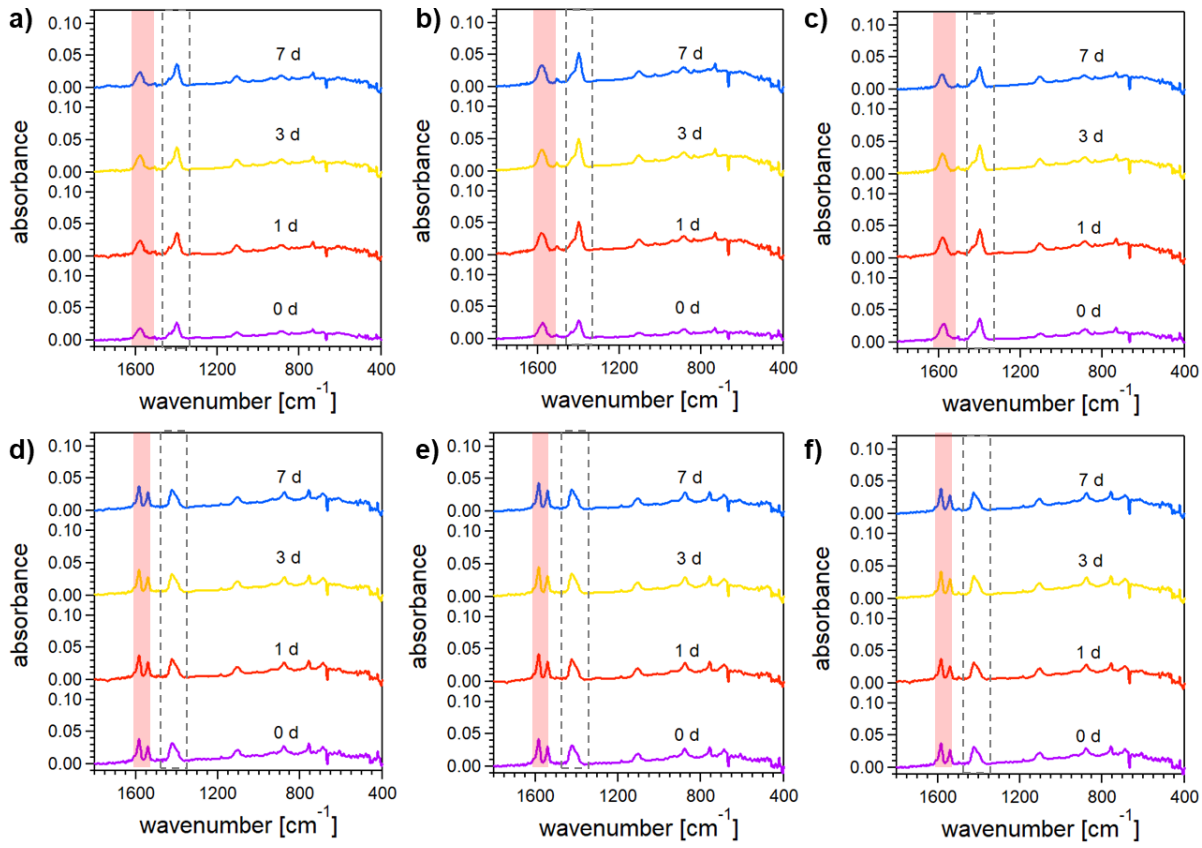


**Fig. S 7:** FTIR spectra of $Cu_2(BDC)_2$ and $Cu_2(BPDC)_2$ films: $Cu_2(BDC)_2$ exposed to **a)** 50% RH, **b)** 80% RH, **c)** liquid $H_2O$, and of $Cu_2(BPDC)_2$ films exposed to **d)** 50% RH, **e)** 80% RH, and **f)** liquid $H_2O$. The region of the asymmetric carboxylate stretching vibration of the MOF films is marked in red and the symmetric carboxylate mode is highlighted in the box with dashed lines.

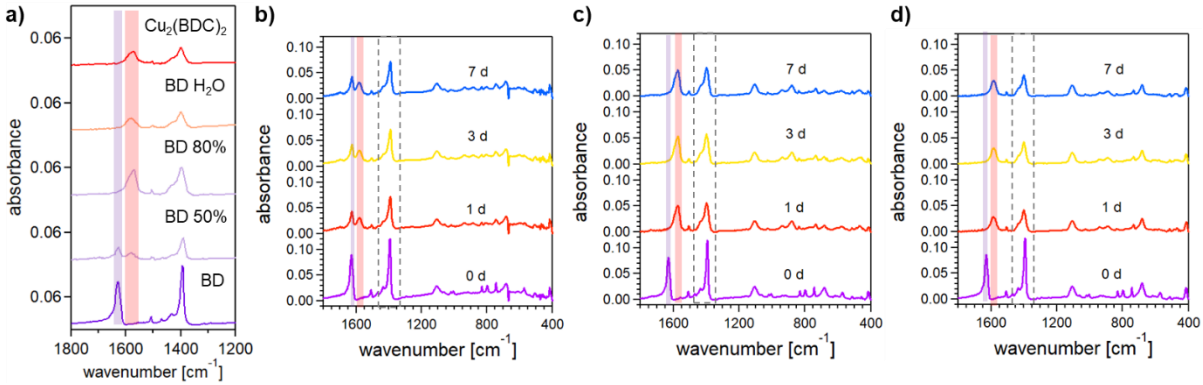


**Fig. S 8:** FTIR spectra of $Cu_2(BDC)_2DABCO$ films: **a)** FTIR spectra showing the evolution of pristine $Cu_2(BDC)_2DABCO$ (BD) to $Cu_2(BDC)_2$ after exposure to different water loadings for 24 h, and FTIR spectra of $Cu_2(BDC)_2DABCO$ films exposed to **b)** 50% RH, **c)** 80% RH, and **d)** liquid $H_2O$. The region of the asymmetric carboxylate stretching vibration of $Cu_2(BDC)_2DABCO$ is marked in purple, the asymmetric carboxylate stretching vibration of $Cu_2(BDC)_2$ is marked in red and the region of the symmetric carboxylate modes for both MOFs is highlighted in the box with dashed lines.

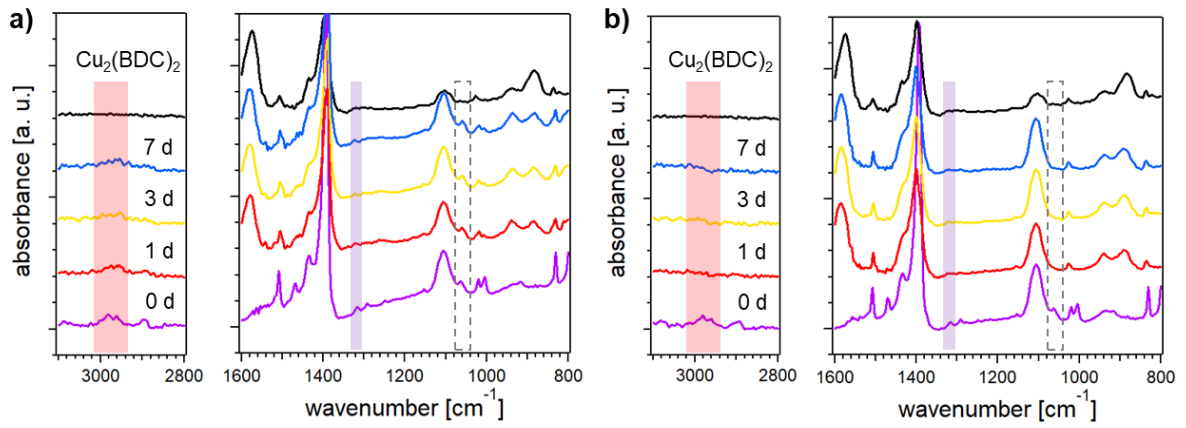


**Fig. S 9:** Vibrational modes of DABCO in FTIR spectra of $Cu_2(BDC)_2DABCO$ films: $Cu_2(BDC)_2DABCO$ films exposed to **a)** 50% RH and **b)** liquid $H_2O$ for 0-7 days, and of $Cu_2(BDC)_2$ as a reference (black graph, depicted and labelled on top). Vibrational bands attributed to the DABCO pillar ligand are highlighted. Red: In-phase $\nu_a(CH_2)$; violet: in-phase $\gamma_t(CH_2)$ and in-phase $\nu_a(NC_3)$; box with dashed lines: in-phase $\nu_a(NC_3)$, $\nu_a$(C–C), and $\gamma_t(CH_2)$; $\nu_a$ = asymmetric stretching, $\gamma_t$ = twisting.[4]

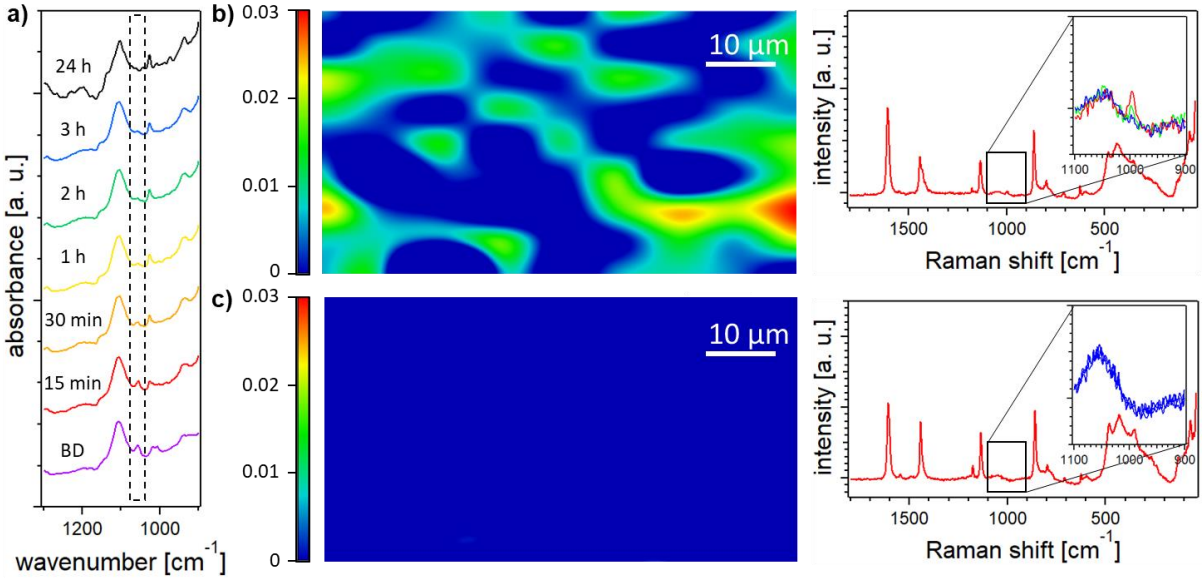


**Fig. S 10:** Vibrational modes of DABCO in FTIR and Raman spectra: **a)** Time-resolved IR-spectra collected for $Cu_2(BDC)_2DABCO$ films exposed to 80% RH (BD corresponds to the pristine MOF before exposure), **b)** Raman map of $Cu_2(BDC)_2DABCO$ films after transformation to $Cu_2(BDC)_2$ at 80% RH, showing an inhomogeneous distribution of released DABCO pillar ligand on the sample surface, and **c)** Raman map of pristine $Cu_2(BDC)_2$, showing no signal in the region of the DABCO-related mode. Raman maps were collected, comprising 62 individual spectra, with a point resolution of 9 x 5 $\mu m^2$ (step size) in a total area of 70 x 40 $\mu m^2$ using a Thermo Scientific DXR2 Raman Microscope equipped with a 532 nm laser. The band at ca. 996 $cm^{-1}$, which is attributed to the v4 ($\nu$CC/$\omega$CH2) mode of DABCO ligand,[5] was used to screen the amount of DABCO on the silicon substrate. The intensity scale for the map was calculated by normalizing the DABCO mode with the C-C stretching mode (ca. 1600 $cm^{-1}$) of the terephthalate. Insets show different color-coded intensities of the 996 $cm^{-1}$ band.

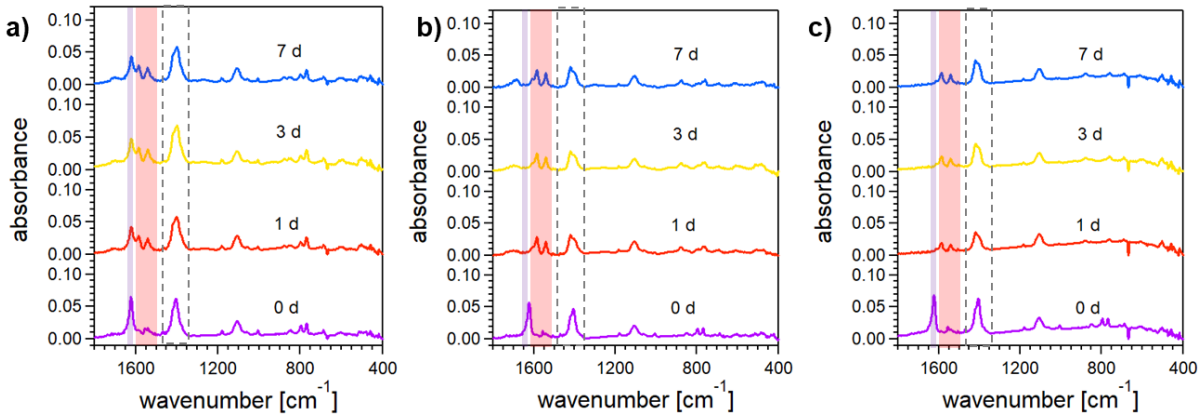


**Fig. S 11:** FTIR spectra of $Cu_2(BPDC)_2DABCO$ films exposed to **a)** 50% RH, **b)** 80% RH, and **c)** liquid $H_2O$. The region of the asymmetric carboxylate stretching vibration of $Cu_2(BPDC)_2DABCO$ is marked in purple, the asymmetric carboxylate stretching vibration of $Cu_2(BPDC)_2$ is marked in red and the region of the symmetric carboxylate modes for both MOFs is highlighted in the box with dashed lines.

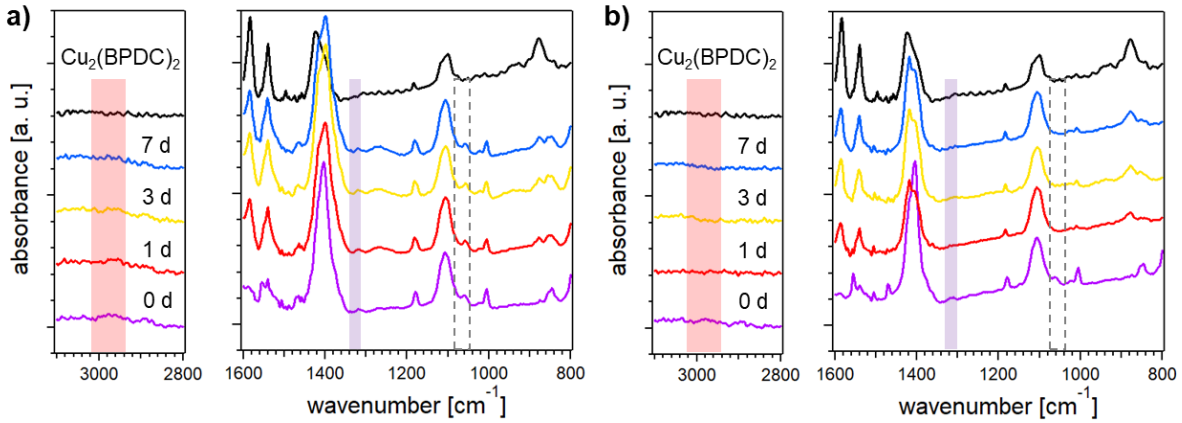


**Fig. S 12:** Vibrational modes of DABCO in FTIR spectra of $Cu_2(BPDC)_2DABCO$ films: $Cu_2(BPDC)_2DABCO$ films exposed to **a)** 50% RH and **b)** liquid $H_2O$ for 0-7 days, and of $Cu_2(BPDC)_2$ as a reference (black graph, depicted and labelled on top). Vibrational bands attributed to the DABCO pillar ligand are highlighted. Red: In-phase $\nu_a(CH_2)$; violet: in-phase $\gamma_t(CH_2)$ and in-phase $\nu_a(NC_3)$; box with dashed lines: in-phase $\nu_a(NC_3)$, $\nu_a(C–C)$, and $\gamma_t(CH_2)$; $\nu_a$ = asymmetric stretching, $\gamma_t$ = twisting.[4]

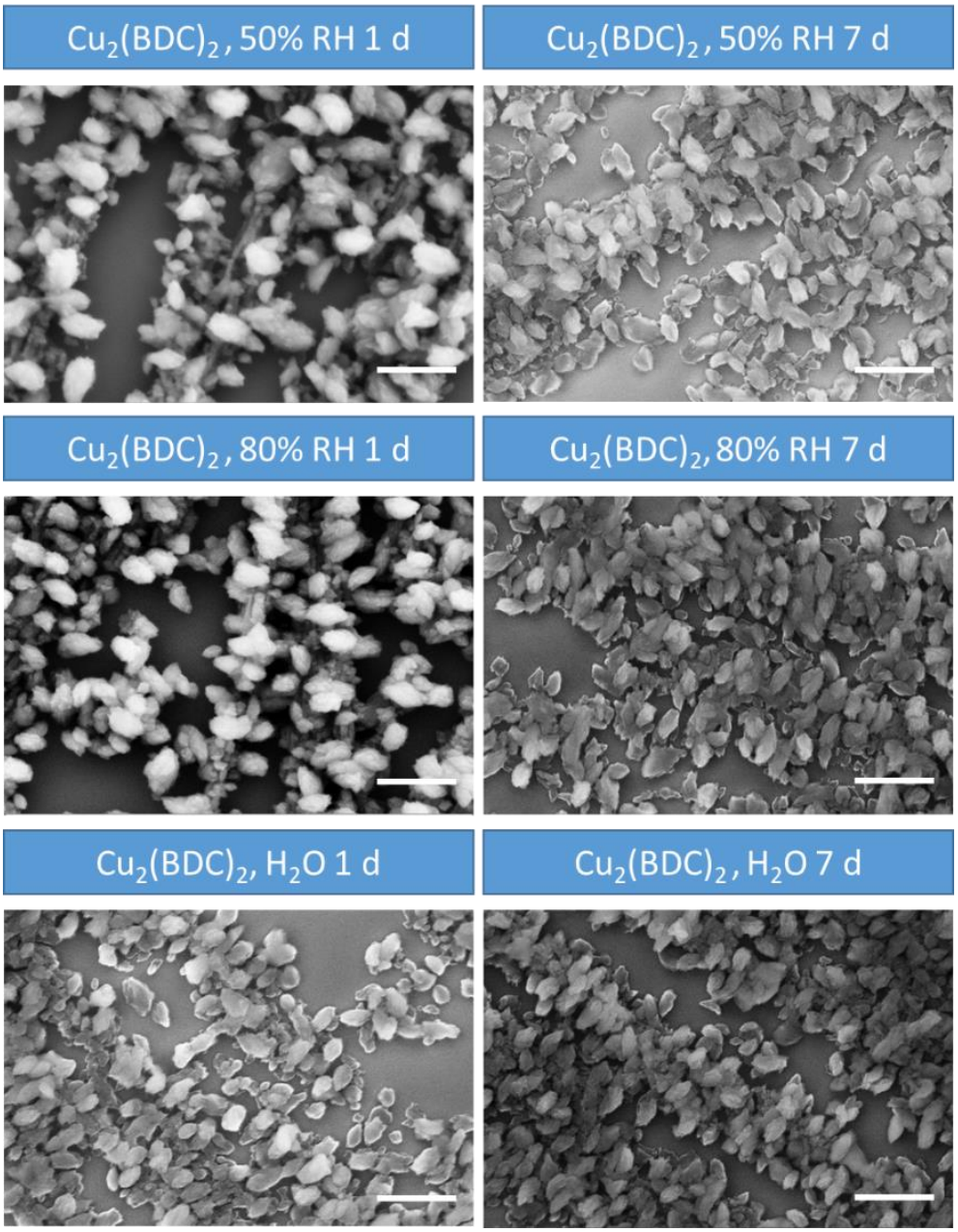


**Fig. S 13:** SEM micrographs of $Cu_2(BDC)_2$ after exposure to different humidity environments. Scale bars represent 500 nm.

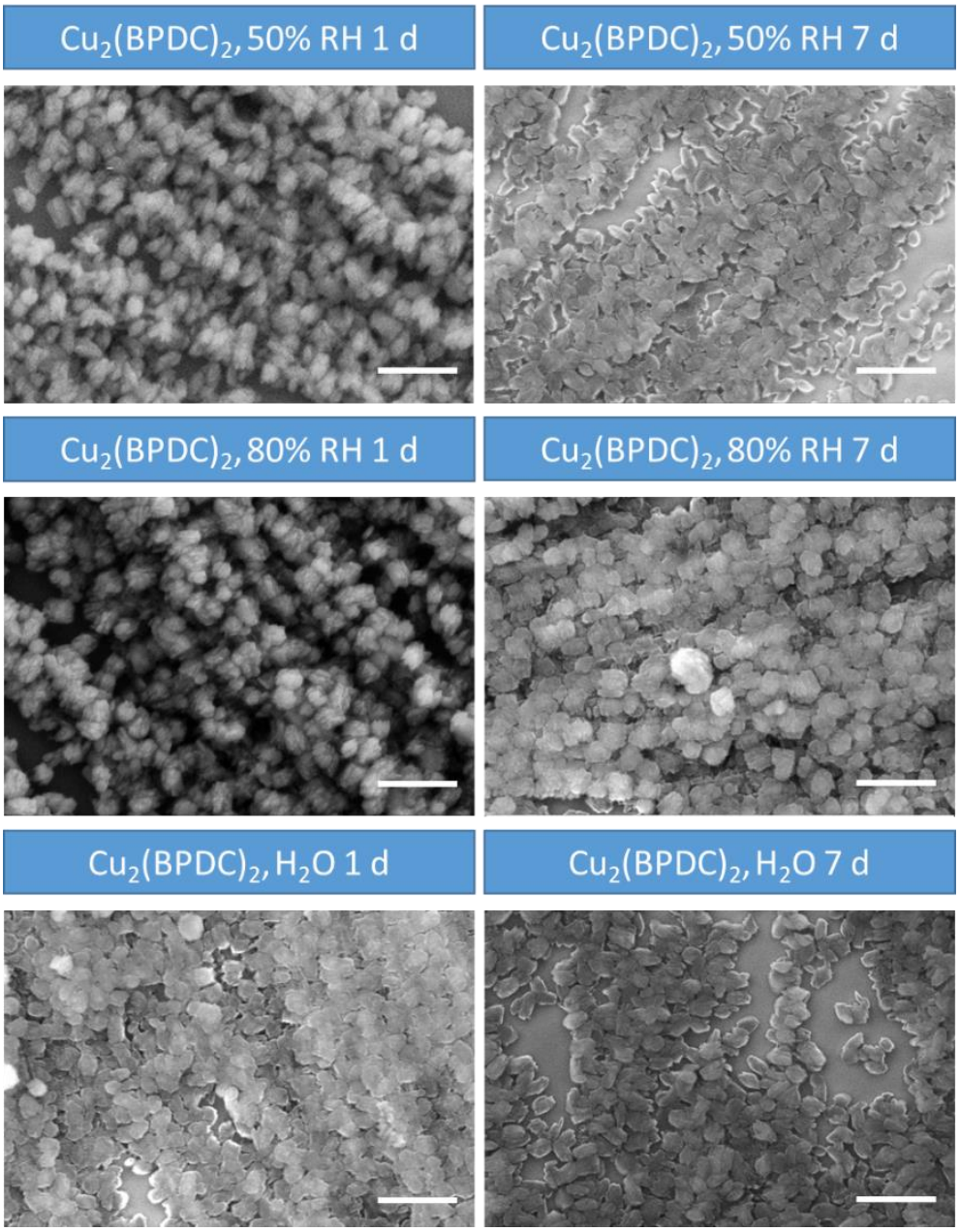


**Fig. S 14:** SEM micrographs of $Cu_2(BPDC)_2$ after exposure to different humidity environments. Scale bars represent 500 nm.

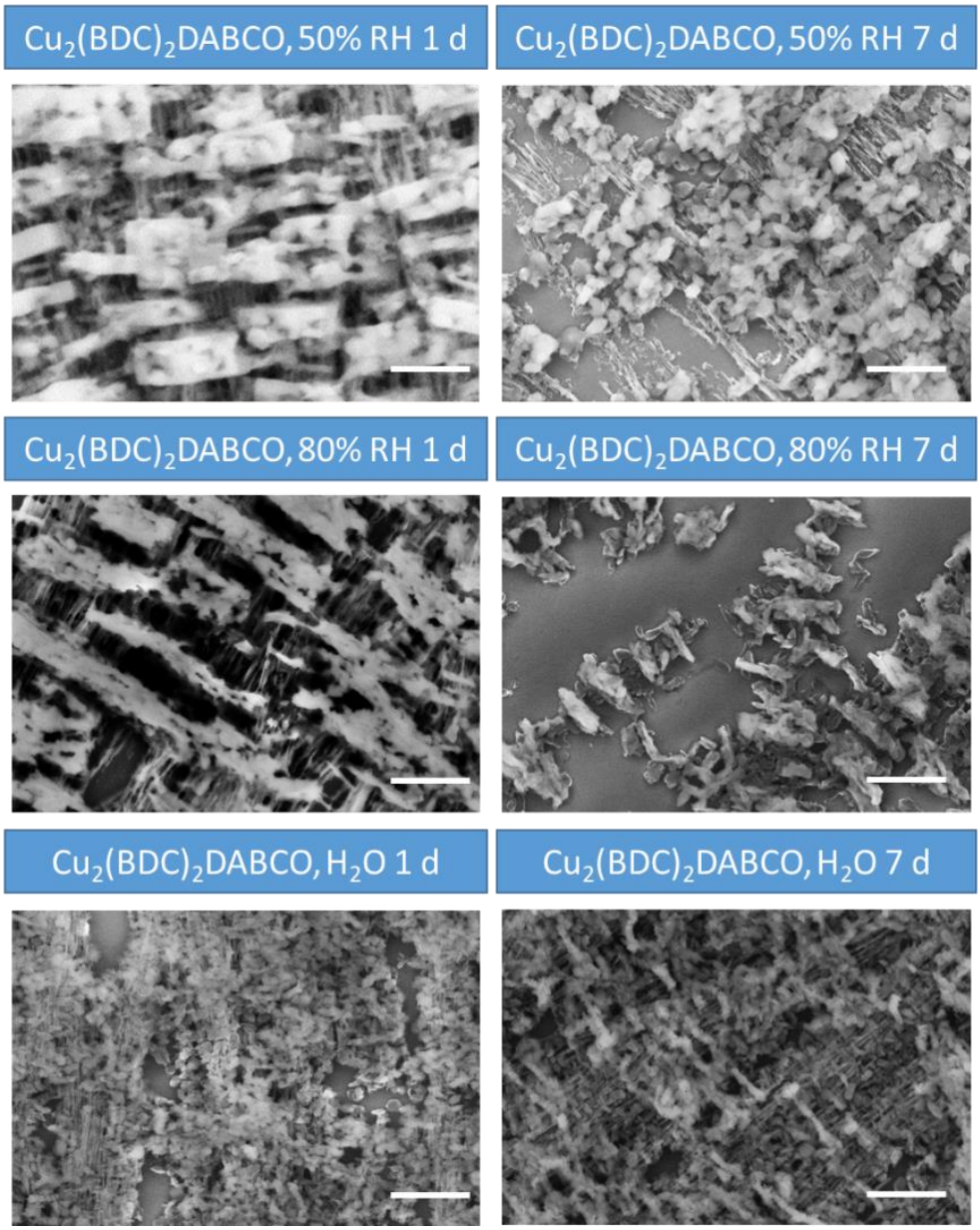


**Fig. S 15:** SEM micrographs of $Cu_2(BDC)_2DABCO$ after exposure to different humidity environments. Scale bars represent 500 nm.

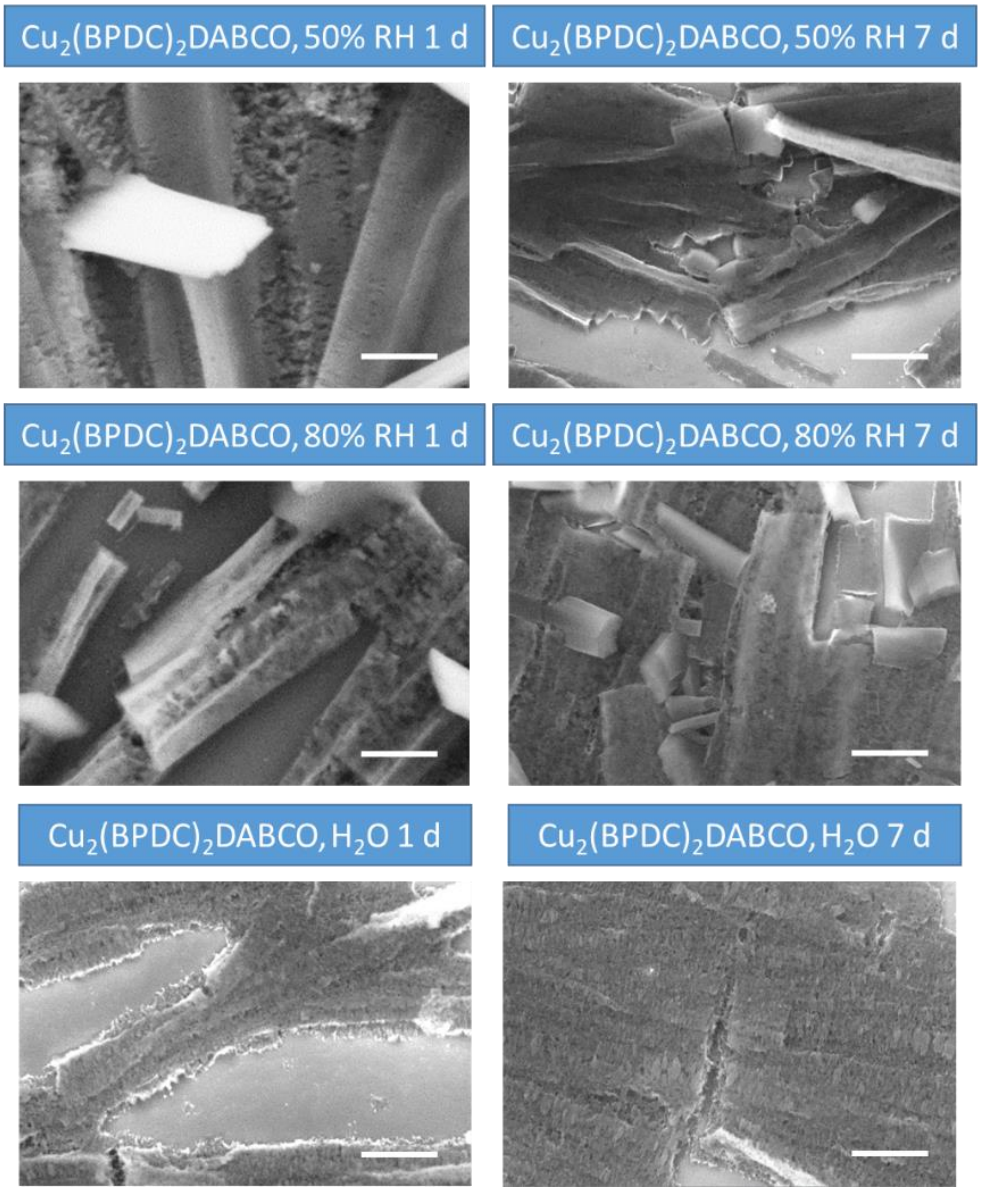


**Fig. S 16:** SEM micrographs of $Cu_2(BPDC)_2DABCO$ after exposure to different humidity environments. Scale bars represent 500 nm.

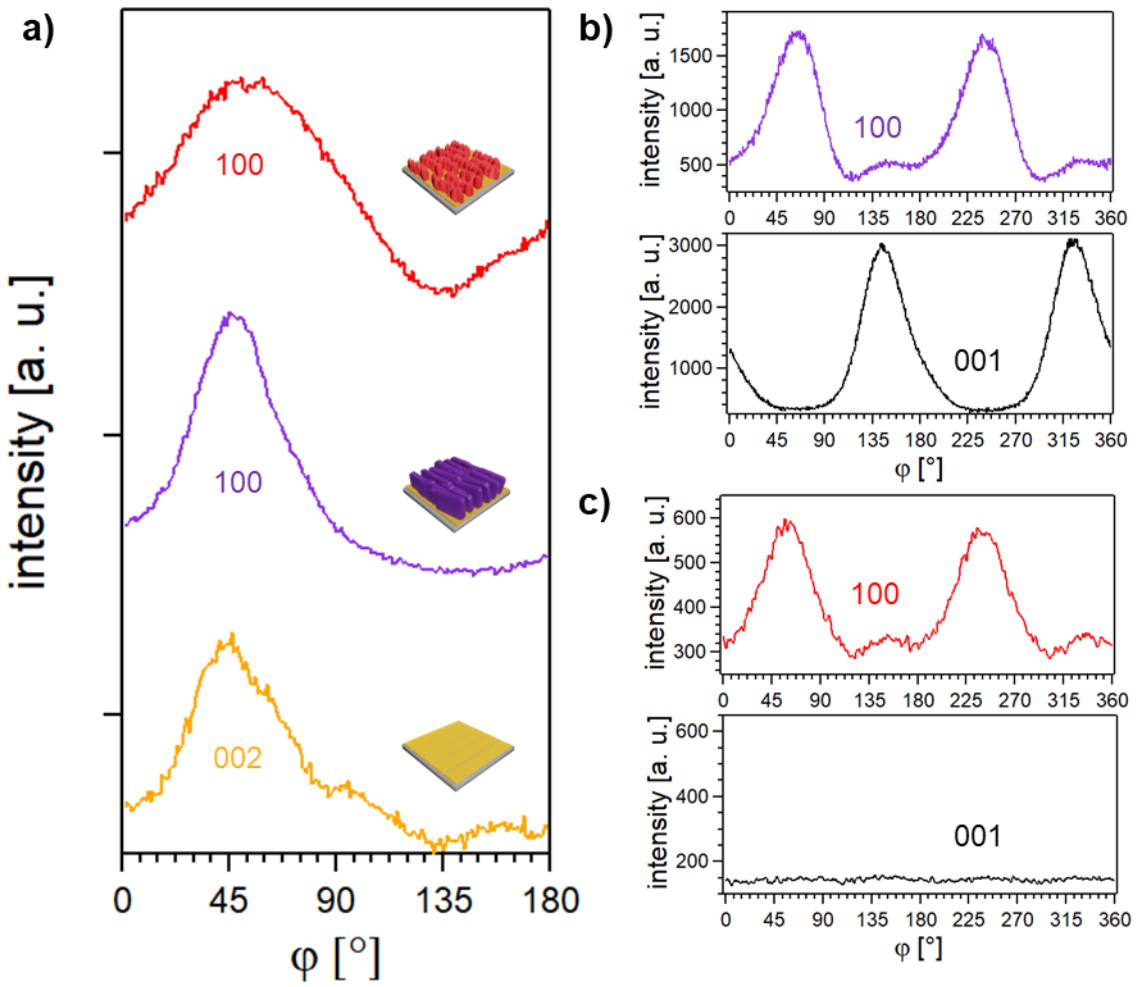


**Fig. S 17:** Azimuthal angle dependence scans: **a)** Intensity profiles of the (002) reflection of residual $Cu(OH)_2$ in the $Cu_2(BDC)_2DABCO$ film (bottom, yellow), of the (100) reflection of pristine $Cu_2(BDC)_2DABCO$ recorded before exposure to $H_2O$ (middle, purple), and of the (100) reflection of newly formed $Cu_2(BDC)_2$ after exposure to $H_2O$ (top, red). Coinciding intensity maxima indicate the heteroepitaxial nature of the growth of $Cu_2(BDC)_2DABCO$ from the $Cu(OH)_2$ substrate and of the subsequent transformation of the 3D framework to $Cu_2(BDC)_2$ in water. The orientation and position of the sample was identical in all azimuthal intensity scans before and after exposure to water. Scans recorded between 0 and 180 °; **b)** intensity profiles of the (100) and (001) reflection of pristine $Cu_2(BDC)_2DABCO$ (top and bottom respectively). Scans recorded between 0 and 360 °; **c)** intensity profile of the (100) reflection of newly formed $Cu_2(BDC)_2$ after exposure of the $Cu_2(BDC)_2DABCO$ film to 80% RH (top), the (001) reflection of $Cu_2(BDC)_2DABCO$ film after transformation, showing a flat line with low intensity which indicates the structural change in the framework through the loss of the DABCO pillar ligand. Scans recorded between 0 and 360 °.

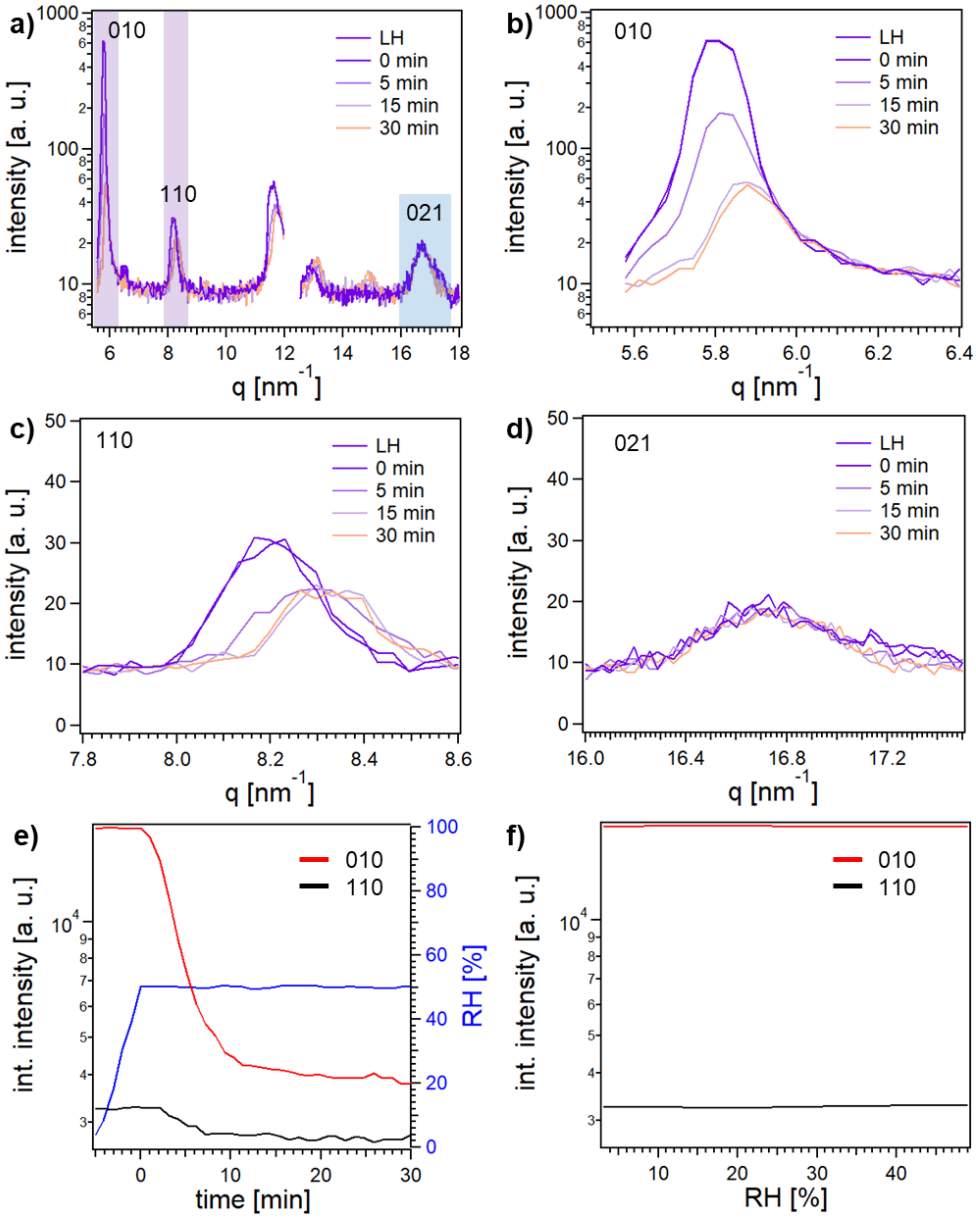


**Fig. S 18:** Selected GIWAXS patterns of the time-resolved experiments of $Cu_2(BDC)_2DABCO$ exposed to 50% RH: **a)** full pattern highlighting the investigated (010) and (110) reflections of $Cu_2(BDC)_2DABCO$ (purple), and the (021) reflection of $Cu(OH)_2$ (blue), **b)** evolution of the (010) reflection of $Cu_2(BDC)_2DABCO$, **c)** evolution of the (110) reflection of $Cu_2(BDC)_2DABCO$, **d)** evolution of the (021) reflection of remaining $Cu(OH)_2$, **e)** integrated intensity of the (010) and (110) reflection of $Cu_2(BDC)_2DABCO$ over time, indicating that the beginning framework hydrolysis requires only 10 min and **f)** integrated intensity of the (010) and (110) reflection of Cu2(BDC)2DABCO during the 10%/min humidity ramp to reach the target value of 50% RH, indicating that the hydrolysis of the framework does not start before 50% RH is reached.

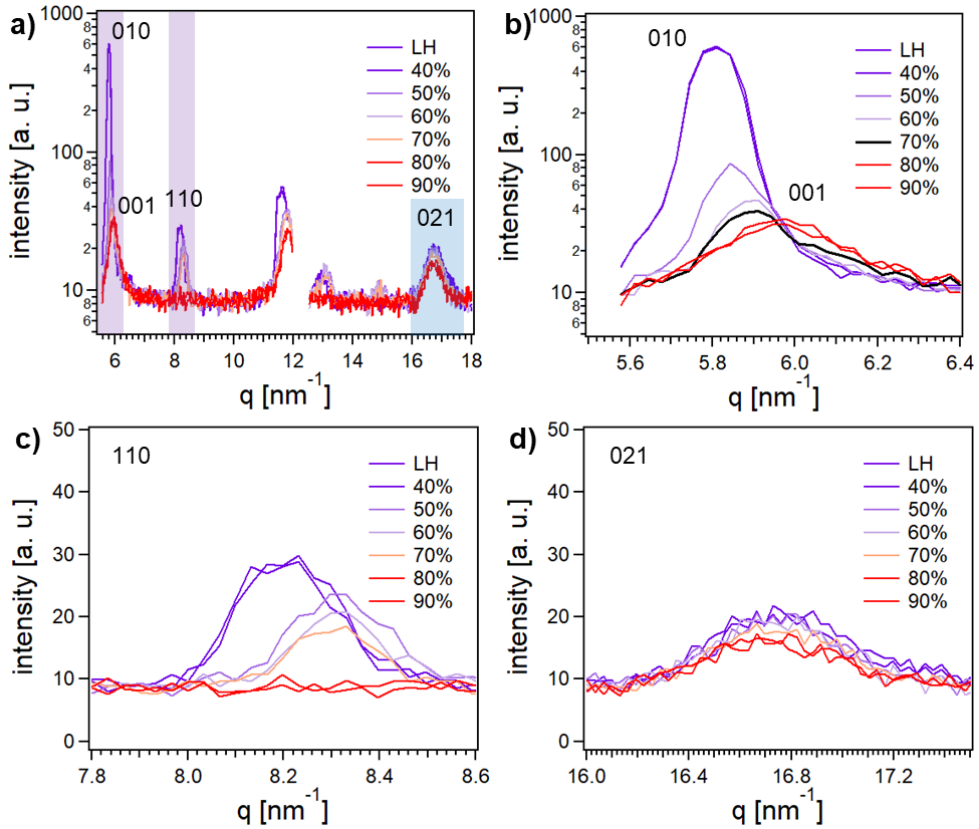


**Fig. S 19:** Selected GIWAXS patterns of the time-resolved experiments of $Cu_2(BDC)_2DABCO$ when increasing the humidity from 5-90% RH by 0.2%/min: **a)** full pattern highlighting the investigated (010) and (110) reflections of $Cu_2(BDC)_2DABCO$ (purple), the (001) reflection of emerging $Cu_2(BDC)_2$, and the (021) reflection of $Cu(OH)_2$ (blue); **b)** evolution of the (010) reflection of $Cu_2(BDC)_2DABCO$ and emergence of the (001) reflection of $Cu_2(BDC)_2$; **c)** decrease of the (110) reflection of $Cu_2(BDC)_2DABCO$ until full degradation of the 3D framework between 70-80% RH; **d)** decrease of the (021) reflection of remaining $Cu(OH)_2$, indicating potential epitaxial growth by reaction of the free BDC linker with the remaining unreacted ceramic precursor material.

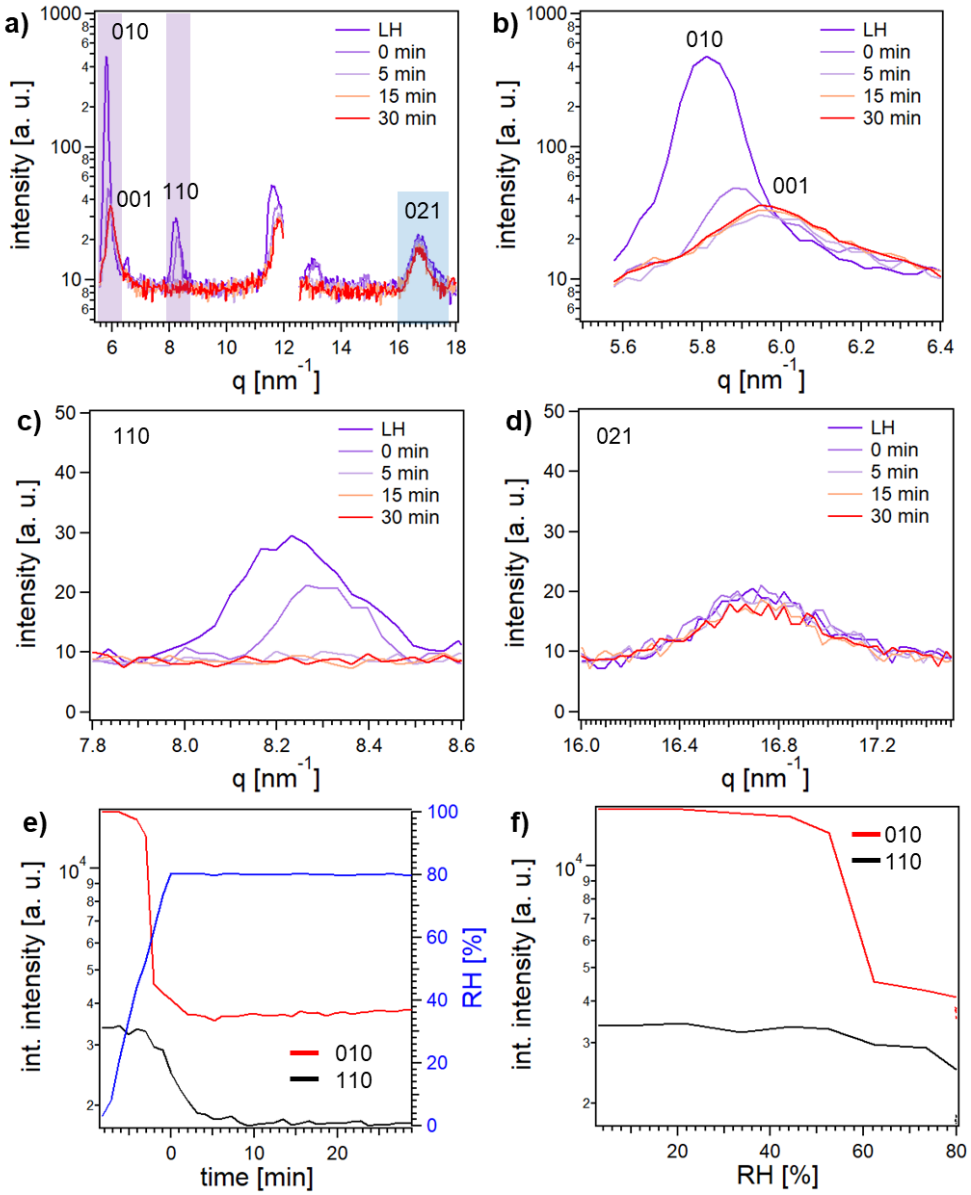


**Fig. S 20:** Selected GIWAXS patterns of the time-resolved experiments of $Cu_2(BDC)_2DABCO$ exposed to 80% RH: **a)** full pattern highlighting the investigated (010) and (110) reflections of $Cu_2(BDC)_2DABCO$ (purple), the (001) reflection of emerging $Cu_2(BDC)_2$, and the (021) reflection of $Cu(OH)_2$ (blue); **b)** evolution of the (010) reflection of $Cu_2(BDC)_2DABCO$ and emergence of the (001) reflection of $Cu_2(BDC)_2$, **c)** decrease of the (110) reflection of $Cu_2(BDC)_2DABCO$, **d)** evolution of the (210) reflection of the remaining $Cu(OH)_2$ layer, **e)** integrated intensity of the (010) and (110) reflection of $Cu_2(BDC)_2DABCO$ over time, indicating that the full transformation from $Cu_2(BDC)_2DABCO$ to $Cu_2(BDC)_2$ requires approx. 20 min (including the humidity ramp to reach the 80% RH target value) and **f)** integrated intensity of the (010) and (110) reflection of $Cu_2(BDC)_2DABCO$ during the 10%/min humidity ramp to reach the target value of 80% RH, indicating the onset of the MOF hydrolysis at 50% RH and of the phase transformation between 60 and 70% RH.

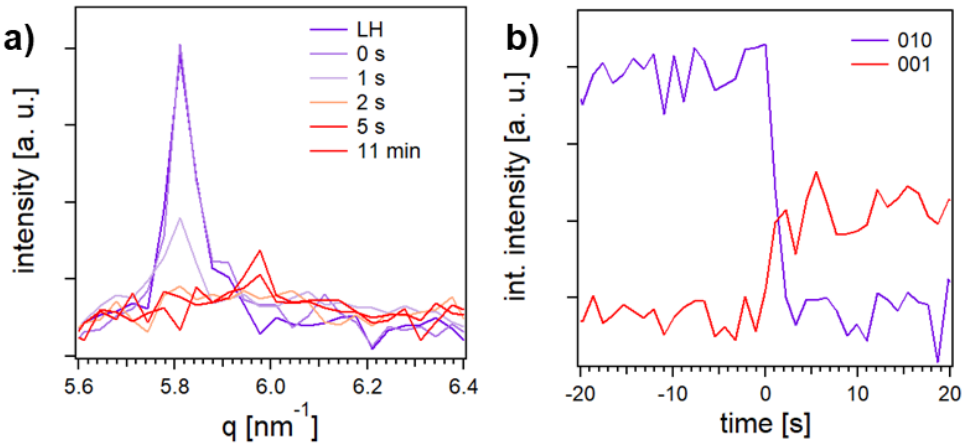


**Fig. S 21:** Selected GIWAXS patterns of the time-resolved experiments of $Cu_2(BDC)_2DABCO$ exposed to water: **a)** decrease of the (010) reflection of $Cu_2(BDC)_2DABCO$ and emergence of the (001) reflection of $Cu_2(BDC)_2$, **b)** integrated intensity of the decreasing (010) reflection of $Cu_2(BDC)_2DABCO$ and of the emerging (001) reflection of $Cu_2(BDC)_2$, indicating that the degradation of the initial 3D MOF occurs simultaneously with the formation of the 2D phase within a few seconds of exposure to liquid $H_2O$. The MOF films used for this experiment were cut to a size of 12 x 3 mm and mounted in the chemical cell under constant $N_2$ flow. Due to the smaller sample size, the signal intensities were reduced, so that weaker reflections, like the (110) reflection of $Cu_2(BDC)_2DABCO$ or the broad (021) reflection of $Cu(OH)_2$, had a very low signal to noise ratio and could not be reliably analysed.

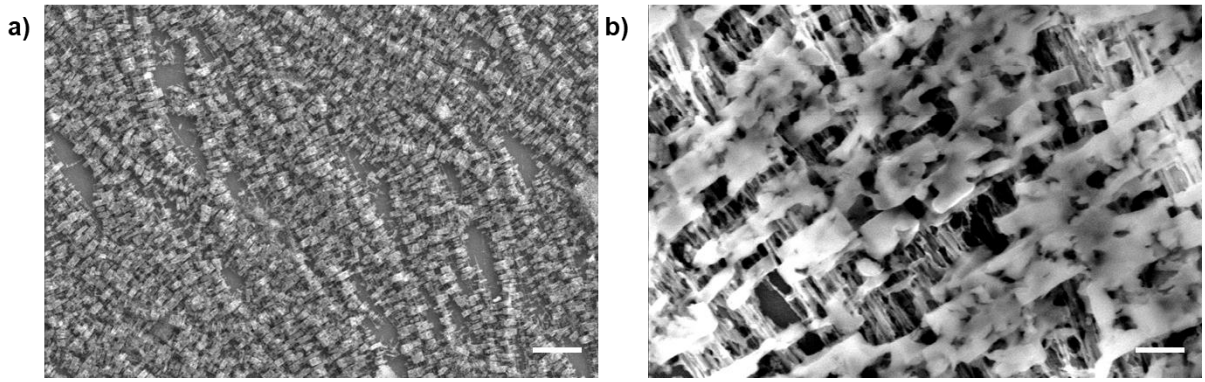


**Fig. S 22:** SEM micrographs of the $Cu_2(BDC)_2DABCO$ film collected after exposure to 50% RH for 30 min during the in situ GIWAXS experiment, **a)** low magnification image, showing the overall distribution and alignment of $Cu_2(BDC)_2DABCO$ (scale bar represents 2 µm), **b)** high magnification image, showing the partially hydrolysed $Cu_2(BDC)_2DABCO$ crystals and unreacted $Cu(OH)_2$ nanobelts underneath (scale bar represents 200 nm). SEM images were recorded shortly after the in situ experiment. The films were stored in $N_2$ until measurement and not exposed to any other solvents or humidity.

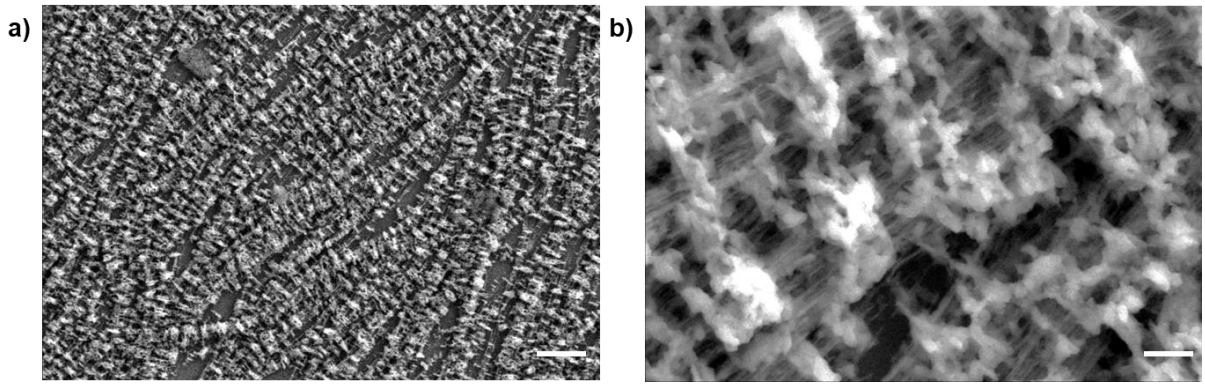


**Fig. S 23:** SEM micrographs of the $Cu_2(BDC)_2DABCO$ film collected after exposure to 80% RH for 30 min during the in situ GIWAXS experiment, **a)** low magnification image, showing that $Cu_2(BDC)_2$ crystals are densely packed where $Cu_2(BDC)_2DABCO$ crystals were previously located (scale bar represents 2 µm), **b)** high magnification image, showing the morphology of $Cu_2(BDC)_2$ and unreacted $Cu(OH)_2$ nanobelts underneath (scale bar represents 200 nm). SEM images were recorded shortly after the in situ experiment. The films were stored in $N_2$ until measurement and not exposed to any other solvents or humidity.

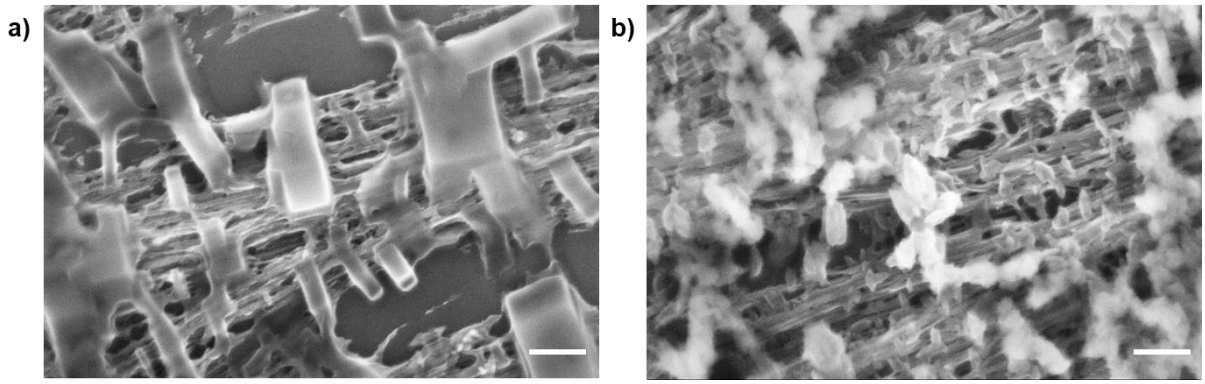


**Fig. S 24:** SEM micrographs of the $Cu_2(BDC)_2DABCO$ films exposed to water: **a)** before exposure to liquid $H_2O$, **b)** after exposure to $H_2O$ for 15 s, showing the crystal morphology of $Cu_2(BDC)_2$. The exposed films show regions with a more concentrated distribution of $Cu_2(BDC)_2$ crystals, probably resulting from the proposed dissolution—recrystallization mechanism. In other areas, $Cu_2BDC_2$ crystals can be seen covering the remaining $Cu(OH)_2$ NBs, possibly resulting from heteroepitaxial growth by reacting with free BDC linker. SEM images were recorded shortly after the in situ experiment. The films were stored in $N_2$ until measurement and not exposed to any other solvents or humidity. Scale bars represent 200 nm.

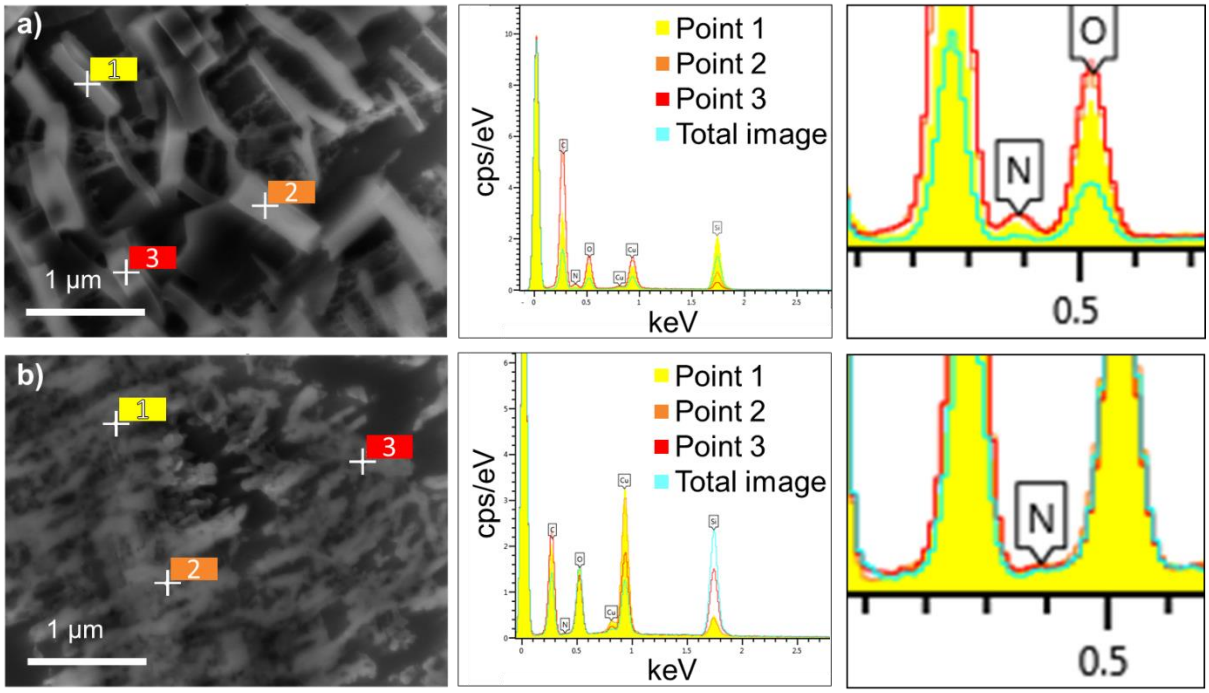


**Fig. S 25:** SEM-EDX spectra obtained from three different points of **a)** pristine $Cu_2(BDC)_2DABCO$ film on Si, showing a nitrogen signal, and of **b)** $Cu_2(BDC)_2$ film on Si after transformation from $Cu_2(BDC)_2DABCO$, showing the loss of the nitrogen signal.

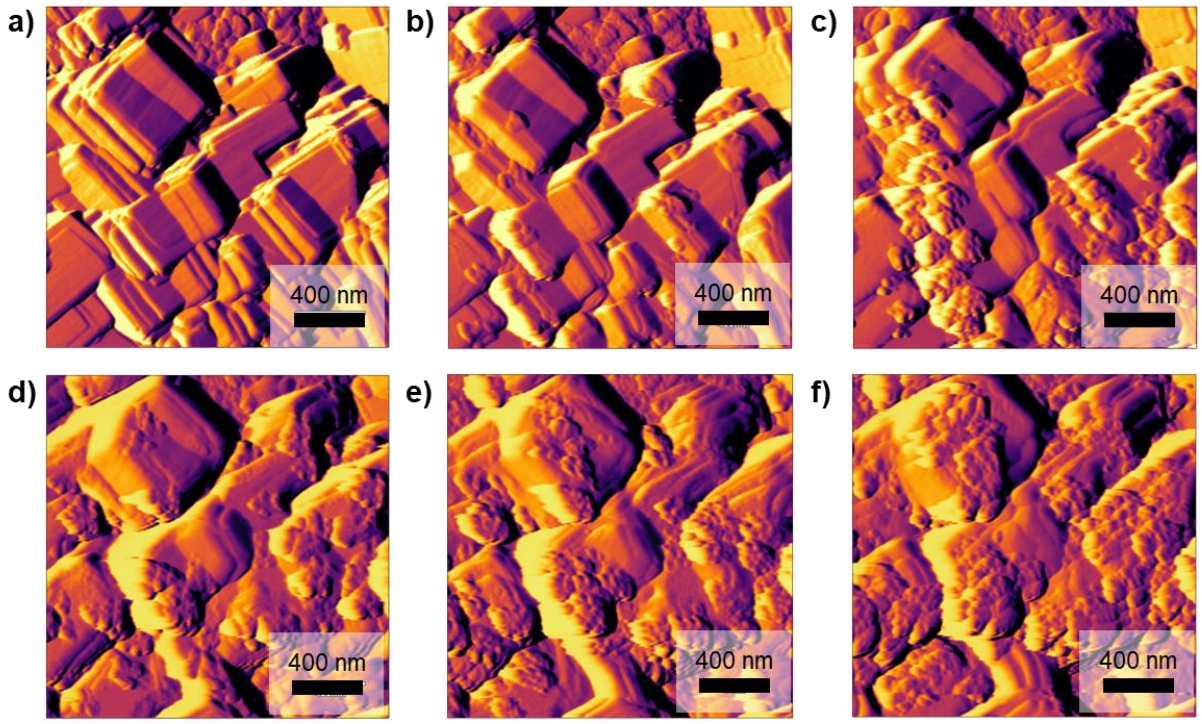


**Fig. S 26:** AFM amplitude images of $Cu_2(BDC)_2DABCO$ during exposure to humid Ar flow (80% RH), collected in tapping mode in an environmental control chamber, for **a)** 0 min, **b)** 5 min, **c)** 20 min, **d)** 50 min, **e)** 75 min, **f)** 100 min.

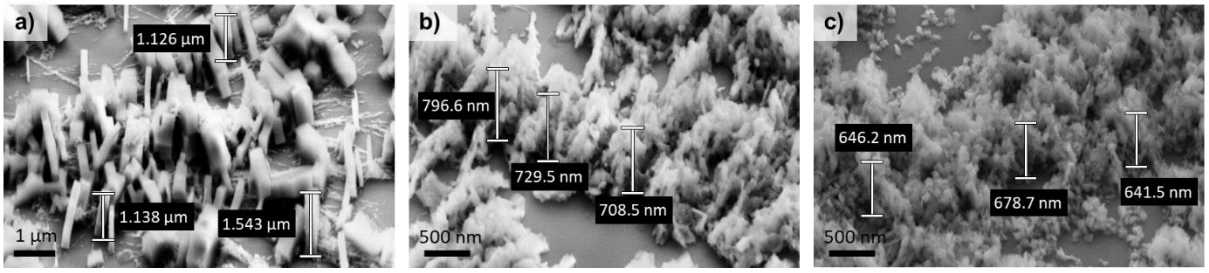


**Fig. S 27:** Estimated film thickness from SEM micrographs of **a)** pristine $Cu_2(BDC)_2DABCO$, **b)** $Cu_2(BDC)_2$ obtained after transformation from $Cu_2(BDC)_2DABCO$ at 80% RH, and **c)** $Cu_2(BDC)_2$ obtained after transformation from $Cu_2(BDC)_2DABCO$ in $H_2O$. Micrographs were recorded at a sample tilting angle of 45° to estimate film thickness.

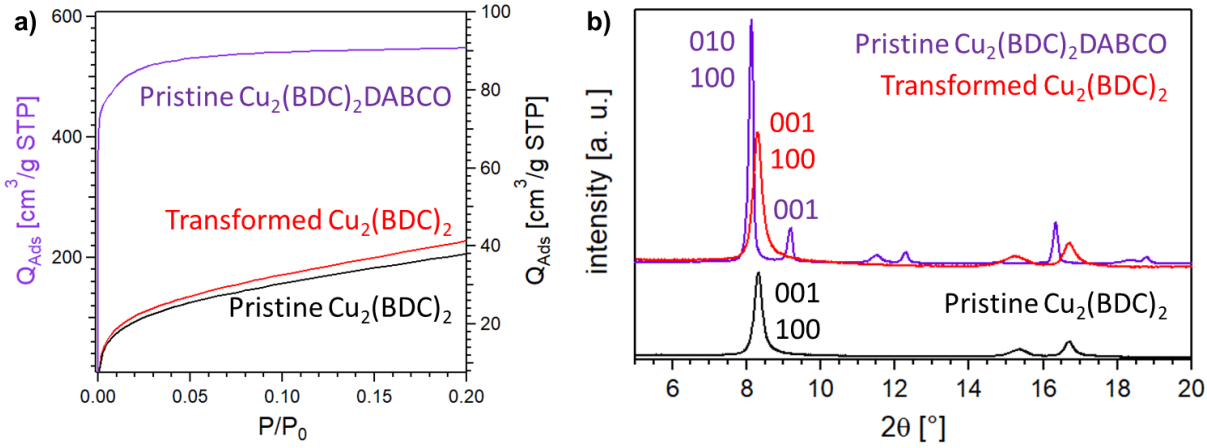


**Fig. S 28:** $N_2$ adsorption data of powdery samples: **a)** micropore range of the adsorption isotherm collected for pristine $Cu_2(BDC)_2DABCO$ (BET surface area = 2200 $m^2/g$) , pristine $Cu_2(BDC)_2$ and transformed $Cu_2(BDC)_2$ ($Q_{Ads}$ of $Cu_2(BDC)_2DABCO$ depicted using the left y-axis, $Q_{Ads}$ of pristine and transformed $Cu_2(BDC)_2$ depicted using the right y-axis). Nitrogen adsorption was performed at 77 K using Micromeritics 3-Flex instrument. Powdery samples were activated at 110 °C for 12 h under vacuum; **b)** PXRD patterns obtained from the powdery samples. For powdery $Cu_2(BDC)_2DABCO$, both the (010)/(100) and the (001) reflection can be observed using the Bragg-Brentano XRD geometry. This can be explained by the random orientation of the crystals in the powdery sample, i. e. out-of-plane contributions can be recorded for all crystallographic planes, including the (001) reflection associated to the length of the DABCO pillar ligand. In the case of powdery $Cu_2(BDC)_2$, the (001)/(100) reflection was recorded at 8.4 °, while the (010) reflection, which corresponds to the distance between the 2D layers, was observed at approx. 15 °. Pristine and transformed powdery $Cu_2(BDC)_2$ show the same PXRD pattern.

## Supporting Tables

**Table S 1:** Average particle size collected from the AFM images with corresponding standard deviation (SD) before and after the MOF-to-MOF transformation.

| | av. length | SD length | av. width | SD width |
|---|---|---|---|---|
| **$Cu_2(BDC)_2DABCO$ (before transf.)** | 530 | 90 | 290 | 40 |
| **$Cu_2(BDC)_2$ (after transf.)** | 110 | 30 | 80 | 6 |

## References


1 B. Marmiroli, B. Sartori, A. R. Kyvik, I. Ratera and H. Amenitsch, *Front. Mater.*, 2021, **8**, 686353.

2 M. Bogar, I. Khalakhan, A. Gambitta, Y. Yakovlev and H. Amenitsch, *J. Power Sources*, 2020, **477**, 229030.

3 H. Amenitsch, M. Rappolt, C. V. Teixeira, M. Majerowicz and P. Laggner, *Langmuir*, 2004, **20**, 4621–4628.

4 V. I. Kovalenko, A. A. Akhmadiyarov, A. E. Vandyukov and A. R. Khamatgalimov, *J. Mol. Struct.*, 2012, **1028**, 134–140.

5 K. Tan, N. Nijem, P. Canepa, Q. Gong, J. Li, T. Thonhauser and Y. J. Chabal, *Chem. Mater.*, 2012, **24**, 3153–3167.